Hindered and modulated rotational states and spectra of adsorbed diatomic molecules

Y. T. Shih
Institute of Electro-Optical Engineering, National Chiao Tung University, Hsinchu, Taiwan, Republic of China

D. S. Chuu*
Department of Electrophysics, National Chiao Tung University, Hsinchu, Taiwan, Republic of China

W. N. Mei
Department of Physics, University of Nebraska at Omaha, Omaha, Nebraska 68182
(Received 17 November 1995; revised manuscript received 29 April 1996)

Both vertical and horizontal adsorption configurations of a diatomic molecule were modeled as the rigid rotor with which the spatial motion was confined by a finite conical well. In addition to the polar hindering potential, a sinusoidal azimuthal modulation, which bears the local symmetry of the adsorption site, was incorporated. Eigenfunctions for different models were expressed analytically in terms of the hypergeometric functions, and eigenvalues were solved numerically. We found that the rotational energy levels exhibit oscillatory behavior when plotted as functions of the hindrance angle. This particular phenomenon was interpreted as the occurrence of resonance transmission of the rotor wave function at certain hindrance condition. We also found that the rotational levels were grouped into bands when the azimuthal modulation strength was increased. The solutions were used to calculate the rotational-state distribution of desorbed molecules, and agreement with the previous experiment was obtained. [S0163-1829(96)07139-1]

I. INTRODUCTION

The hindered-rotation problem is an important topic in the study of the following topics: the internal rotation of a molecule which can be modeled as a frame with attached tops;[1–5] the overall rotation of a molecule which is bounded inside a crystal;[6–8] and the overall rotation of a molecule which is adsorbed on a solid surface.[9–23] Examples of the first case can be found in the organic molecules, e.g., in methyl alcohol. When a molecule is bounded inside a crystal or adsorbed on a solid surface, owing to the molecule-molecule or molecule-surface interaction, the rotational motion of the molecule is usually frustrated, and thus is definitely different from that of a free rotor. Hence a thorough study of the states and energies of the hindered rotation is crucial to an understanding of the spectra of molecules and molecular crystals, and the dynamics of adsorption and desorption.

The first evidence for the hindered rotation of an adsorbed molecule was the observation of orthopara separation factors of the adsorbed hydrogen and deuterium.[9,13,24,25] Sandler[9] first showed that orthohydrogen can be adsorbed more strongly than parahydrogen when it is physically adsorbed on TiO_2 and activated charcoal. Subsequently, it was also demonstrated that paradeuterium as well as orthohydrogen can be adsorbed more strongly on alumina.[13,24,25] Sandler suggested that the mechanism of the preferential adsorption might be caused by the hindered rotation of adsorbed molecules. Preferential adsorption on selective surfaces made it possible to prepare pure orthohydrogen and paradeuterium.[24–26]

Recently, the rotational motion of a molecule which interacts with a solid surface has attracted increasing interest. Many experimental studies such as surface neutron scattering,[13] surface infrared spectroscopy,[21] electron-energy-loss spectroscopy,[27,28] electron- and photon-stimulated desorption,[19,22,29,30] thermal desorption,[31–33] and gas-surface inelastic scattering[34–38] provided fruitful information about the rotational states of adsorption systems. For example, the measured rotational-state distributions of molecules scattered or desorbed from surfaces were found to exhibit a temperature-independent non-Boltzmann feature, which can be attributed to hindered rotations of adsorbed molecules.[14–16,22,23]

On the other hand, for theoretical studies, many simplified models for surface potentials were proposed to simulate the hindered rotational motion,[10,14,17,19,23] and a deeper theoretical understanding was acquired. Among those studies, Gadzuk and co-workers suggested an infinite-conical-well model,[14–17] in which the rotor is only allowed to rotate within the well region. Rotational-state energy spectra for both vertical and horizontal adsorption configurations were obtained. Together with a sudden unhindrance approximation, they interpreted the non-Boltzmann properties of the rotational-state distributions of molecules desorbed from surfaces. However, the infinite-conical-well model potential is, by construction, more suitable for strong molecule-surface interaction cases because it precludes completely the probability of a rotor appearing outside the cone. Therefore, in the weaker interaction cases a finite conical well which allows the rotor to rotate with polar angle lying outside the well is preferable. Furthermore, it is difficult to deduce the molecule-surface interaction strength from the experimental data when comparing them with the theoretical results obtained from solving a hard-wall hindering potential. In our previous work,[23] we presented a finite-conical-well model to

study the rotational-state energy spectra of a vertically adsorbed diatomic molecule. It was found that the rotational energy levels of the soft-wall-hindered rotor exhibit oscillatory behavior when plotted as functions of the hindrance angle. By using the analogy of the Kronig-Penney model, we showed this particular behavior, which does not appear in the hard-wall case, is clearly the manifestation of the rotational invariance of the present model. In this paper, we extend our previous study to the horizontal configuration. In addition, we include, to both vertical and horizontal configurations, the periodic azimuthal modulation from which the effect of the local symmetry of the adsorption site can be incorporated. Landman *et al.*[17] studied similar effects by using a periodic square-well potential in their infinite-conical-well model. In order to imitate more closely the real situation around the adsorbed molecule, we adopted potentials with sinusoidal oscillation from which analytical solutions can be obtained. The potential models and mathematical method we developed in our works can be generalized straightforwardly to investigate the internal rotational states in molecules and the rotational spectra of molecules in crystalline solids.

II. MODELS AND SOLUTIONS

The Schrödinger equation for the hindered molecular rotation in spherical coordinates can be expressed as

$$\left[\frac{1}{\sin\theta}\frac{\partial}{\partial\theta}\left(\sin\theta\frac{\partial}{\partial\theta}\right)+\frac{1}{\sin^2\theta}\frac{\partial^2}{\partial\phi^2}+E^{\mathrm{rot}}-V^{\mathrm{hin}}(\theta,\phi)\right]\Psi^{\mathrm{rot}}_{\nu,\mu}(\theta,\phi)=0, \tag{1}$$

where E^{rot} and V^{hin} are the rotational energy and the hindering potential energy. For convenience, the energies are expressed in the unit of the molecular rotational constant $B=\hbar^2/2I$, where I is the molecular moment of inertia with respect to its center of rotation. $\Psi^{\mathrm{rot}}_{\nu,\mu}$ is the angular wave function of the hindered molecule. The subscripts ν and μ represent the quantum numbers arising from the dependence of the hindering potential upon θ and ϕ.

In accordance with the objective of modeling the problem by solvable potentials, we express $V^{\mathrm{hin}}(\theta,\phi)$ in the following specific form to ensure separation of variables:[17,39]

$$V^{\mathrm{hin}}(\theta,\phi)=\left[V(\theta)+\frac{W(\phi)}{\sin^2\theta}\right]. \tag{2}$$

Hence the angular wave function can be written as a product of two factors:

$$\Psi^{\mathrm{rot}}_{\nu,\mu}(\theta,\phi)=\Theta_{\nu,\mu}(\theta)\Phi_{\mu}(\phi), \tag{3a}$$

where Φ_μ and $\Theta_{\nu,\mu}$ satisfy the following equations:

$$\left[\frac{d^2}{d\phi^2}+\mu^2-W(\phi)\right]\Phi_{\mu}(\phi)=0 \tag{3b}$$

and

$$\left[\frac{1}{\sin\theta}\frac{d}{d\theta}\left(\sin\theta\frac{d}{d\theta}\right)+\nu(\nu+1)-V(\theta)-\frac{\mu^2}{\sin^2\theta}\right]\Theta_{\nu,\mu}(\xi)=0, \tag{3c}$$

where $\xi=\cos\theta$. In deriving Eq. (3c), the rotational energy has been expressed in terms of the rotational quantum number ν:

$$E^{\mathrm{rot}}=\nu(\nu+1), \tag{4}$$

which makes an obvious connection with the limit of free rotation.

In Eq. (3b), $W(\phi)$ is the periodic azimuthal modulation arising from the local symmetry of the adsorption site. One can imitate more closely to the real situation around the adsorbed molecule by assuming $W(\phi)$ in a sinusoidal oscillation form:[1,6,19]

$$W(\phi)=W_0\left[\frac{1-\cos(N\phi)}{2}\right], \tag{5}$$

where N is an integer characterizing the azimuthal periodicity of the site, and W_0 is the height of the modulation barrier. Thus Eq. (3b) becomes

$$\left[\frac{d^2}{d\phi^2}+a-2q\cos(N\phi)\right]\Phi_{\mu}(\phi)=0, \tag{6a}$$

where

$$a=\mu^2-\frac{W_0}{2},\quad q=-\frac{W_0}{4}. \tag{6b}$$

Equation (6a) is just the Mathieu's equation.[41] From the Floquet-Bloch theorem and the requirement of single value of wave function, one can express $\Phi_\mu(\phi)$ in terms of the Fourier series as

$$\Phi_{\mu}(\phi)=\sum_{s=-\infty}^{\infty}C_s\exp[i(m+sN)\phi], \tag{7a}$$

where m and s are integers. Inserting (7a) into (6a), one can obtain the following recursion relation for determining the Fourier coefficients:

$$C_{s-1}+C_{s+1}=\tau_s C_s,\quad \tau_s\equiv\frac{a-(m+sN)^2}{q}, \tag{7b}$$

and then derive a continued fraction relation

$$\tau_0-\frac{1}{\tau_{-1}-}\frac{1}{\tau_{-2}-}\frac{1}{\tau_{-3}-}\cdots-\frac{1}{\tau_1-}\frac{1}{\tau_2-}\frac{1}{\tau_3-}\cdots=0, \tag{7c}$$

If $m=0$, $\Phi_\mu(\phi)$ can bear definite parity, then the coefficient C_0 has to vanish for the odd-parity states. Thus Eq. (7c) is only suitable for the even-parity states and has to be modified as

$$\tau_1-\frac{1}{\tau_2-}\frac{1}{\tau_3-}\frac{1}{\tau_4-}\cdots=0 \tag{7d}$$

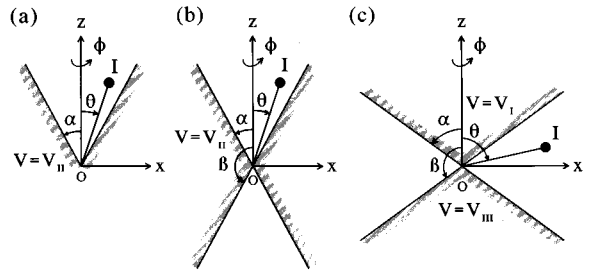

FIG. 1. Schematics of the finite-conical-well hindering potential for (a) vertical adsorption configuration with potential parameters $V_{\mathrm{I}}=0$; and $V_{\mathrm{II}}=V_{\mathrm{III}}>0$; (b) vertical adsorption configuration with potential parameters $V_{\mathrm{I}}=V_{\mathrm{III}}=0$, $V_{\mathrm{II}}>0$, and $\beta=\pi-\alpha$; and (c) horizontal adsorption configuration with potential parameters $V_{\mathrm{II}}=0$, $V_{\mathrm{I}}=V_{\mathrm{III}}>0$, and $\beta=\pi-\alpha$. O presents the center of rotation, and I is the molecular moment of inertia with respect to its center of rotation.

for the odd states. The eigenvalue μ^2 of Eq. (6a) for given m and W_0 can be determined numerically by solving Eqs. (7c) and (7d).

Figure 1 illustrates the hindering potentials used to model the constraint upon the rotational motion of an adsorbed diatomic molecule either in the vertical or horizontal configuration. The rotors are confined within a conical domain bounded at certain polar angles. However, unlike the previous studies,[14–17] we used soft potential walls, i.e., finite heights in the barrier regions, to study the adsorption behaviors at the weaker molecule-surface interaction range. General form for the polar hindering potential $V(\theta)$ corresponding to both the vertical and horizontal configurations is

$$V(\theta)=\begin{cases} V_{\mathrm{I}}, & 0\leqslant\theta<\alpha \\ V_{\mathrm{II}}, & \alpha\leqslant\theta\leqslant\beta \\ V_{\mathrm{III}}, & \beta<\theta\leqslant\pi, \end{cases} \tag{8}$$

where V_{I}, V_{II}, and V_{III} represent the barrier heights for region I ($0\leqslant\theta<\alpha$), region II ($\alpha\leqslant\theta\leqslant\beta$), and region III ($\beta<\theta\leqslant\pi$), respectively.

For the vertical adsorption configuration,[22,42,43] the molecular axis is preferred to be perpendicular to the surface, therefore one can assume that $V(\theta)$ is minimum about $\theta=0$; thus $V_{\mathrm{I}}=0$ and $V_{\mathrm{II}}>0$. If the adsorbed molecule rotates about its center of mass, there are two cases to be considered. The first case is that $V(\theta)$ has only one minimum at $\theta=0$, thus $V_{\mathrm{II}}=V_{\mathrm{III}}>0$ [see Fig. 1(a)]. This geometry can also simulate an adsorbed diatomic molecule, in which one end might be clamped to a surface via a chemical bond, rotating about its attached atom. The second case is that $V(\theta)$ has two minima at $\theta=0$ and $\theta=\pi$, thus $V_{\mathrm{II}}>V_{\mathrm{III}}>0$. If the adsorbed molecule is homonuclear, then $V(\theta)$ is symmetrical with respect to the $\theta=\pi/2$ plane, thus $V_{\mathrm{I}}=V_{\mathrm{III}}=0$ and $\beta=\pi-\alpha$ [see Fig. 1(b)].

On the other hand, in the horizontal configuration,[44,45] the molecular axis is preferred to parallel the surface; therefore one can assume that $V(\theta)$ is minimum about $\theta=\pi/2$, thus $V_{\mathrm{II}}=0$, $V_{\mathrm{I}}>0$, and $V_{\mathrm{III}}>0$. If the adsorbed molecule is homonuclear, one can further simplify the model by imposing $V_{\mathrm{I}}=V_{\mathrm{III}}$ and $\beta=\pi-\alpha$ [see Fig. 1(c)]. In short, the horizontal configuration is suitable to describe practically most of the physisorbed diatomic molecules.

Since in our models $V(\theta)$ in each region is independent of θ, we can define a parameter ν' as

$$\nu'(\nu'+1)=\nu(\nu+1)-V(\theta), \tag{9}$$

which is independent of θ in each region, then Eq. (3c) in each region is just the associated Legendre equation[40,41] with degree ν' and order μ:

$$(1-\xi^2)\frac{d^2\Theta_{\nu,\mu}}{d\xi^2}-2\xi\frac{d\Theta_{\nu,\mu}}{d\xi}+\left[\nu'(\nu'+1)-\frac{\mu^2}{1-\xi^2}\right]\Theta_{\nu,\mu}=0, \tag{10}$$

where $\xi=\cos\theta$. Usually, the solutions of the above equation are expressed in terms of $P^{\mu}_{\nu'}$ and $Q^{\mu}_{\nu'}$, the associated Legendre functions of the first kind and second kinds. However, the numerical treatments of those functions near their singularities, i.e., $\xi=\pm1$, are rather unstable. A more convenient alternate is to express the solutions of the above equation in terms of the hypergeometric functions around their singular points $\xi=1$ and -1.[23] Now expressing $\Theta_{\nu,\mu}(\xi)$ as

$$\Theta_{\nu,\mu}(\xi)=(1-\xi^2)^{|\mu|/2}\mathcal{W}(\xi), \tag{11}$$

and substituting it into Eq. (10), one obtains the standard form of the hypergeometric equation[40,41] for $\mathcal{W}$:

$$\eta(1-\eta)\frac{d^2\mathcal{W}}{d\eta^2}+[c-(a+b+1)\eta]\frac{d\mathcal{W}}{d\eta}-ab\mathcal{W}=0, \tag{12a}$$

where $\eta=(1-\xi)/2$, and

$$\begin{aligned} a&=|\mu|-\nu', \\ b&=1+|\mu|+\nu', \\ c&=1+|\mu|. \end{aligned} \tag{12b}$$

Therefore, the linearly independent solutions of Eq. (10) in the neighborhood of the singular points $\xi=\pm1$ can be expressed as[41]

$$\mathcal{P}_{(\pm1)}(\nu',\mu,\xi)=(1-\xi^2)^{|\mu|/2}F\left(|\mu|-\nu',1+|\mu|+\nu';1+|\mu|;\frac{1\mp\xi}{2}\right), \tag{13a}$$

$$\mathcal{Q}_{(\pm1)}(\nu',\mu,\xi)=(1-\xi^2)^{-|\mu|/2}F\left(-|\mu|-\nu',1-|\mu|+\nu';1-|\mu|;\frac{1\mp\xi}{2}\right), \tag{13b}$$

where $F(a,b;c;z)$ is the hypergeometric function. One can easily note that, for unspecified ν' and μ, $\mathcal{P}_{(\pm1)}$ converges at $\xi=\pm1$ but diverges at $\xi=\mp1$, while $\mathcal{Q}_{(\pm1)}$ diverges at $\xi=\pm1$. Thus the solution for Eq. (10) in three different potential regions can be written as

$$\Theta_{\nu,\mu}(\xi)=\begin{cases} C_{\mathrm{I},\nu,\mu}\mathcal{P}_{(+1)}(\nu'_{\mathrm{I}},\mu,\xi), & \cos\alpha<\xi\leqslant 1 \\ C_{\mathrm{II},\nu,\mu}\mathcal{P}_{(+1)}(\nu'_{\mathrm{II}},\mu,\xi)+D_{\mathrm{II},\nu,\mu}\mathcal{Q}_{(+1)}(\nu'_{\mathrm{II}},\mu,\xi), & \cos\beta\leqslant\xi\leqslant\cos\alpha \\ C_{\mathrm{III},\nu,\mu}\mathcal{P}_{(-1)}(\nu'_{\mathrm{III}},\mu,\xi), & -1\leqslant\xi<\cos\beta, \end{cases} \tag{14a}$$

where ν'_{I}, ν'_{II}, and ν'_{III} are defined as

$$\begin{aligned} \nu'_{\mathrm{I}}(\nu'_{\mathrm{I}}+1)&=\nu(\nu+1)-V_{\mathrm{I}}, \\ \nu'_{\mathrm{II}}(\nu'_{\mathrm{II}}+1)&=\nu(\nu+1)-V_{\mathrm{II}}, \\ \nu'_{\mathrm{III}}(\nu'_{\mathrm{III}}+1)&=\nu(\nu+1)-V_{\mathrm{III}}. \end{aligned} \tag{14b}$$

In order to determine ν, one has to match the boundary conditions at $\xi_1=\cos\alpha$ and $\xi_2=\cos\beta$, which yield

$$\begin{aligned} &[\mathcal{P}_{(+1)}(\nu'_{\mathrm{II}},\mu,\xi_1)\mathcal{P}'_{(+1)}(\nu'_{\mathrm{I}},\mu,\xi_1)-\mathcal{P}_{(+1)}(\nu'_{\mathrm{I}},\mu,\xi_1)\mathcal{P}'_{(+1)}(\nu'_{\mathrm{II}},\mu,\xi_1)] \\ &\quad\times[\mathcal{P}_{(-1)}(\nu'_{\mathrm{III}},\mu,\xi_2)\mathcal{Q}'_{(+1)}(\nu'_{\mathrm{II}},\mu,\xi_2)-\mathcal{Q}_{(+1)}(\nu'_{\mathrm{II}},\mu,\xi_2)\mathcal{P}'_{(-1)}(\nu'_{\mathrm{III}},\mu,\xi_2)] \\ &\quad+[\mathcal{P}_{(+1)}(\nu'_{\mathrm{I}},\mu,\xi_1)\mathcal{Q}'_{(+1)}(\nu'_{\mathrm{II}},\mu,\xi_1)-\mathcal{Q}_{(+1)}(\nu'_{\mathrm{II}},\mu,\xi_1)\mathcal{P}'_{(+1)}(\nu'_{\mathrm{I}},\mu,\xi_1)] \\ &\quad\times[\mathcal{P}_{(-1)}(\nu'_{\mathrm{III}},\mu,\xi_2)\mathcal{P}'_{(+1)}(\nu'_{\mathrm{II}},\mu,\xi_2)-\mathcal{P}_{(+1)}(\nu'_{\mathrm{II}},\mu,\xi_2)\mathcal{P}'_{(-1)}(\nu'_{\mathrm{III}},\mu,\xi_2)]=0, \end{aligned} \tag{15}$$

for nontrivial solutions, where $\mathcal{P}'_{(\pm1)}=d\mathcal{P}_{(\pm1)}/d\xi$, and $\mathcal{Q}'_{(\pm1)}=d\mathcal{Q}_{(\pm1)}/d\xi$. For given μ, α, β, V_{I}, V_{II}, and V_{III}, one can determine ν by solving Eq. (15) numerically, and thus obtain the rotational energies from Eq. (4).

In the absence of azimuthal modulation, the parameter $c=1+|\mu|=1+|m|$ can only have integer values because of the requirement of single value of the azimuthal wave function. Equations (14a) and (15) are still valid if $\mathcal{Q}_{(+1)}(\nu',m,\xi)$ is replaced by

$$\begin{aligned} \mathcal{Q}_{(+1)}(\nu',m,\xi)=(1-\xi^2)^{|m|/2}\times\Bigg\{ & F\left(|m|-\nu',1+|m|+\nu';1+|m|;\frac{1-\xi}{2}\right)\ln\left(\frac{1-\xi}{2}\right) \\ &+\sum_{n=1}^{\infty}\frac{(|m|-\nu')_n(1+|m|+\nu')_n}{(1+|m|)_n n!}\left(\frac{1-\xi}{2}\right)^n[\psi(|m|-\nu'+n)-\psi(|m|-\nu')+\psi(1+|m|+\nu'+n) \\ &-\psi(1+|m|+\nu')-\psi(1+|m|+n)+\psi(1+|m|)-\psi(1+n)+\psi(1)] \\ &-\sum_{n=1}^{|m|}\frac{(n-1)!(-|m|)_n}{(1-|m|+\nu')_n(-|m|-\nu')_n}\left(\frac{1-\xi}{2}\right)^{-n}\Bigg\}, \end{aligned} \tag{16}$$

where $\psi(a)$ is the digamma function.

Some special cases can be considered in the following: for the vertical configuration with $V_{\mathrm{I}}=0$ and $V_{\mathrm{II}}=V_{\mathrm{III}}$, i.e., there is only one conical well, the entire polar space is divided into two regions. The wave functions are

$$\Theta_{\nu,\mu}(\xi)=\begin{cases} C_{\mathrm{I},\nu,\mu}\mathcal{P}_{(+1)}(\nu,\mu,\xi), & \cos\alpha\leqslant\xi\leqslant 1 \\ C_{\mathrm{II},\nu,\mu}\mathcal{P}_{(-1)}(\nu'_{\mathrm{II}},\mu,\xi), & -1\leqslant\xi<\cos\alpha, \end{cases} \tag{17a}$$

and the eigenvalues can be obtained from solving the following equation:

$$\mathcal{P}_{(+1)}(\nu,\mu,\xi_1)\mathcal{P}'_{(-1)}(\nu'_{\mathrm{II}},\mu,\xi_1)-\mathcal{P}'_{(+1)}(\nu,\mu,\xi_1)\mathcal{P}_{(-1)}(\nu'_{\mathrm{II}},\mu,\xi_1)=0. \tag{17b}$$

As $V_{\mathrm{II}}\to\infty$, Eqs. (17a) and (17b) can be reduced to

$$\Theta_{\nu,\mu}(\xi)=\begin{cases} C_{\mathrm{I},\nu,\mu}\mathcal{P}_{(+1)}(\nu,\mu,\xi), & \cos\alpha\leqslant\xi\leqslant 1 \\ 0, & -1\leqslant\xi<\cos\alpha \end{cases} \tag{18a}$$

and

$$\mathcal{P}_{(+1)}(\nu,\mu,\xi_1)=0. \tag{18b}$$

On the other hand, for the horizontal configuration, that is with $V_{\mathrm{II}}=0$, but both V_{I} and $V_{\mathrm{III}}\to\infty$, the wave functions can be expressed as

$$\Theta_{\nu,\mu}(\xi)=\begin{cases}0, & \cos\alpha\leqslant\xi\leqslant 1\\ C_{\mathrm{II},\nu,\mu}\mathcal{P}_{(+1)}(\nu,\mu,\xi)+D_{\mathrm{II},\nu,\mu}\mathcal{Q}_{(+1)}(\nu,\mu,\xi), & \cos\beta\leqslant\xi\leqslant\cos\alpha\\ 0, & -1\leqslant\xi<\cos\beta,\end{cases} \tag{19a}$$

and the eigenvalues can be obtained by solving

$$\mathcal{P}_{(+1)}(\nu,\mu,\xi_1)\mathcal{Q}_{(+1)}(\nu,\mu,\xi_2)-\mathcal{P}_{(+1)}(\nu,\mu,\xi_2)\times\mathcal{Q}_{(+1)}(\nu,\mu,\xi_1)=0. \tag{19b}$$

One can note that Eqs. (18a), (18b), (19a), and (19b) are exactly the same as the results obtained in Refs. 14 and 17.

For the special case that no restrictive conical well exists, i.e., $V(\theta)=0$, the wave function is

$$\Theta_{\nu,\mu}(\xi)=C_{\nu,\mu}\mathcal{P}_{(+1)}(\nu,\mu,\xi),\quad -1\leqslant\xi\leqslant 1, \tag{20a}$$

which diverges at $\xi=-1$ $(\theta=\pi)$ unless $|\mu|-\nu=-n$, where n is a non-negative integer. This renders the hypergeometric function representing $\mathcal{P}_{(+1)}(\nu,\mu,\xi)$ terminates at finite terms. Thus for given μ, the eigenvalues ν are

$$\nu=|\mu|+n,\quad n=0,1,2,\ldots\ . \tag{20b}$$

By making use of the transformation formulas of the hypergeometric functions,[41] the total angular part wave functions can be written as

$$\Psi^{\mathrm{rot}}_{\nu,\mu}(\theta,\phi)=C_{\nu,\mu}P_{\nu}^{-|\mu|}(\cos\theta)\Phi_{\mu}(\phi). \tag{21}$$

Furthermore, if the azimuthal modulation potential is absent, $\mu=m$ is also an integer. Therefore, for a given m, the eigenvalues $\nu=l$ are integers which are equal or greater than $|m|$:

$$l=|m|+n,\quad n=0,1,2,\ldots, \tag{22a}$$

and the corresponding wave functions can be written as

$$\Psi^{\mathrm{rot}}_{l,m}(\theta,\phi)=C_{l,m}P_{l}^{m}(\cos\theta)\exp(im\phi). \tag{22b}$$

This is exactly the familiar result of a free-space rotor.

III. RESULTS AND DISCUSSION

A. Hindered rotational energy levels

For the vertical adsorption configuration, we set $V_{\mathrm{I}}=0$ and $V_{\mathrm{II}}>0$ in Eq. (8). For the simplest case $V_{\mathrm{II}}=V_{\mathrm{III}}$, as shown in Fig. 1(a), if the azimuthal modulation is absent, the wave functions are given by Eq. (17a) with $\mu=m=$integer. The eigenvalues can be obtained from solving Eq. (17b) numerically. The results were discussed in our previous paper.[23] Now let us consider another hindering potential case, i.e., $V_{\mathrm{III}}=0$ and $\beta=\pi-\alpha$ for the vertical configuration. In this case, $V(\theta)$ is just a double potential well in the polar angle space as shown in Fig. 1(b). The low-lying rotational energy levels for such hindering potential without azimuthal modulation are presented in Fig. 2 as functions of cone opening angle α for three different potential barrier heights, namely, $V_{\mathrm{II}}=5$, 20, and 80. From Fig. 2, one can find that when α is decreased from $\pi/2$ to zero the level energy corresponding to the lth free rotor level increases from $E^{\mathrm{rot}}=l(l+1)B$ to $E^{\mathrm{rot}}=l(l+1)B+V_{\mathrm{II}}B$. The rotational levels above the barrier also exhibit oscillatory behavior as results of the single conical well. From Fig. 2, one can note that for a given potential barrier height V_{II}, the rotational levels with the same value of $n(\equiv l-|m|)$ exhibit the same behavior as α changes, and the levels with the same n but larger $|m|$ are always higher than those with smaller $|m|$. This is a common feature for both the vertical and horizontal rotors, as we will see below. Therefore, the rotational energy levels can be classified into several families according to the values of n, and it is convenient to denote the calculated rotational energy levels by the pair of numbers, (n,m). Figure 2 shows that the number of oscillations (i.e., the number of $dE^{\mathrm{rot}}/d\alpha\approx 0$ in the region $0<\alpha<\pi/2$) of the levels, belonging to the nth family in the region of $0<\alpha<\pi/2$, is equal to $[n/2]$, where $[x]$ denotes the largest integer $\leqslant x$. Figure 2 also shows that lower-energy levels of the hindered rotor for a given value of $|m|$ are nearly degenerate in pairs for larger potential barrier heights and medium open angles. This degeneracy is the general feature of a symmetric double well structure.[46,47] One can note that the higher the barrier height is, the more obvious the degeneracy of levels is.

For the horizontal adsorption configuration, the polar hindering potential is chosen as $V_{\mathrm{II}}=0$, $V_{\mathrm{I}}=V_{\mathrm{III}}$, and

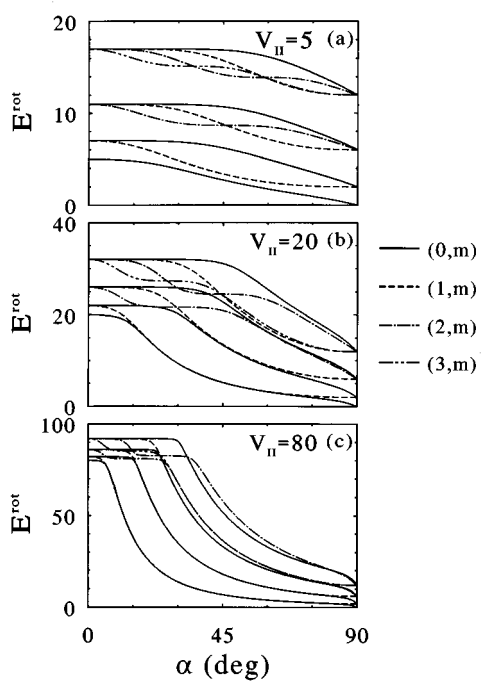

FIG. 2. Low-lying rotational energy levels (in units of $B=\hbar^2/2I$) of a vertically hindered rotor [see Fig. 1(b)] as functions of the hindrance angle α (in degrees) with $\beta=180°-\alpha$ for potential barrier heights $V_{\mathrm{I}}=V_{\mathrm{III}}=0$ and (a) $V_{\mathrm{II}}=5$, (b) $V_{\mathrm{II}}=20$, and (c) $V_{\mathrm{II}}=80$.

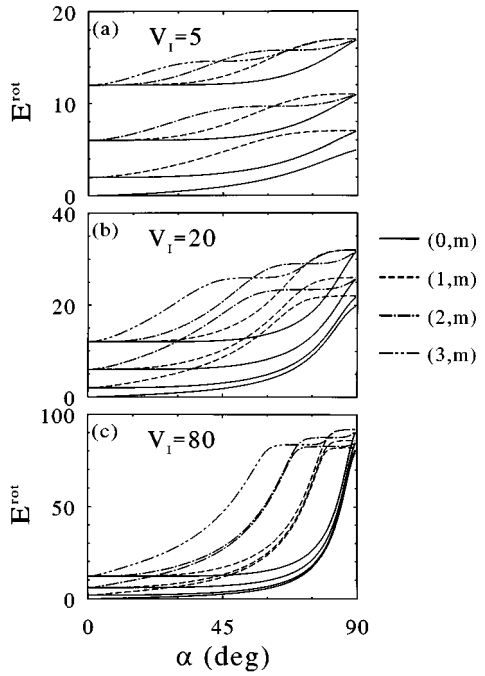

FIG. 3. Low-lying rotational energy levels (in units of $B=\hbar^2/2I$) of a horizontally hindered rotor [see Fig. 1(c)] as functions of the hindrance angle α (in degrees) with $\beta=180°-\alpha$ for potential barrier heights $V_{II}=0$ and (a) $V_I=V_{III}=5$, (b) $V_I=V_{III}=20$, and (c) $V_I=V_{III}=80$.

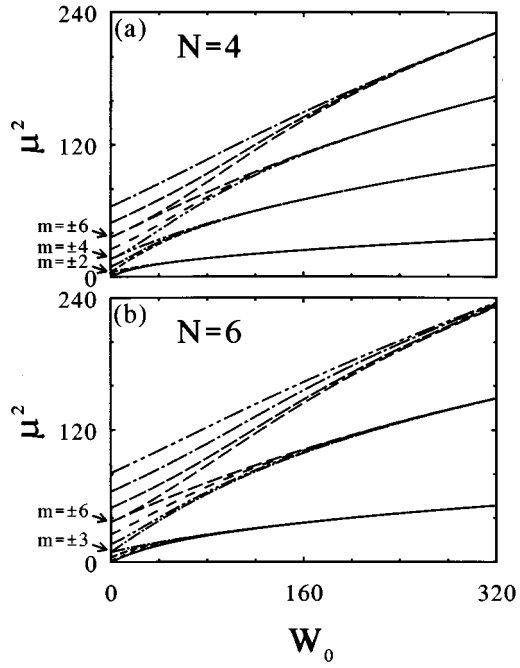

FIG. 4. Azimuthal quantum number μ^2 as functions of azimuthal modulation potential barrier height W_0 for different values of m. The results are presented for symmetric numbers (a) $N=4$, and (b) $N=6$.

$\beta=\pi-\alpha$ in Eq. (8), as shown in Fig. 1(c). One can note from Figs. 1(b) and 1(c) that this case is just the geometry complement of the symmetric vertical conical well. The calculated low-lying rotational energy levels for such a hindering potential without azimuthal modulation are shown in Fig. 3 as functions of the hindrance angle α for three different potential-barrier heights, namely, $V_I=5$, 20, and 80. As in the case of vertical configuration, the rotational energies of the horizontal rotor increase as the spatial localization is increased. When α changes from zero to $\pi/2$, the energy increases from $E^{\rm rot}=l(l+1)B$ to $E^{\rm rot}=l(l+1)B+V_IB$. For the smaller barrier height, e.g., $V_I=5$, the energy levels can be categorized into different groups in accordance with the quantum numbers l of the free rotor. But for larger barrier heights, e.g., $V_I=20$, the levels start to intersect with each others. If the barrier height is sufficiently large, e.g., $V_I=80$, the rotational levels become to group into different families as α approaches $\pi/2$. However, in the case of finite potential barriers the leakage of the rotor wave function outside the well is possible. Therefore, when the conical well region is very small, i.e., α is close to $\pi/2$, the molecule does not behave like a two-dimensional plan rotor; instead, it behaves like a three-dimensional rotor again. From Fig. 3, one can note that as in the cases of vertically hindered rotors, the energy levels of the soft-wall horizontal rotor also exhibit oscillatory behavior when the level energies are plotted as functions of hindrance angle. The number of oscillation of the levels belonging to the nth family in the region of $0<\alpha<\pi/2$ is equal to $[n/2]$.

The oscillatory behavior of $E^{\rm rot}$ can be ascribed to the phenomenon of the resonance transmission.[23] If the hindering potential is absent, the solution is the associated Legendre function P_l^m The number of nodes of the solution in the region $0<\theta<\pi$ is $n=l-|m|$. When the hindering potential is present, the wave function is distorted by the potential wall; however, the number of nodes does not change. When the well reduces to the situation that the potential wall is located on the node position of the wave function, the resonance transmission occurs. Therefore, the amplitude of the rotor wave function inside the well reaches a minimum, and $E^{\rm rot}$ is not sensitive to the reduction of the well, i.e., $dE^{\rm rot}/d\alpha\approx 0$. As the conical well reduces further, the node position of the wave function does not locate on the potential wall, and the resonance transmission disappears until the next coincidence of potential wall and node position of wave function occurs. Therefore, the number of oscillations of the rotational level is related to the number of nodes of the solution. For the single vertical conical-well potential [Fig. 1(a)], the numbers of oscillation of the rotational levels as α changes from zero to π are n. On the other hand, for the symmetric conical-well potential [Figs. 1(b) and 1(c)], the numbers of oscillation of the rotational levels as α changes from zero to $\pi/2$ are $[n/2]$.

B. Azimuthal modulation effect

The effect of increasing W_0 upon azimuthal quantum numbers μ^2 for different values of m can be obtained by solving Eqs. (7c) and (7d). The results are presented in Fig. 4 for $N=4$ and 6. One can note the progressive splitting for m at Brillouin-zone edge values (i.e., $|m|=2,4,6,\ldots$, for $N=4$ or $|m|=3,6,9,\ldots$, for $N=6$) and greater banding of μ^2 as the height of the azimuthal barrier W_0 is increased.

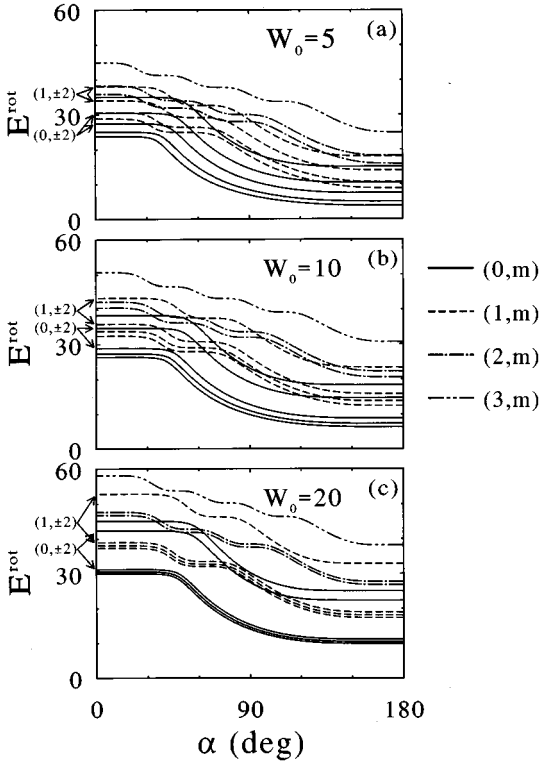

FIG. 5. Low-lying rotational energy levels (in units of $B=\hbar^2/2I$) of a vertically hindered rotor [see Fig. 1(a) for $V_{\mathrm{I}}=0$, and $V_{\mathrm{II}}=V_{\mathrm{III}}=20$] as functions of the hindrance angle α (in degrees) for azimuthal modulation potential barrier heights (a) $W_0=5$, (b) $W_0=10$, and (c) $W_0=20$. The azimuthal modulation is sinusoidal with fourfold symmetry ($N=4$). The (n,m) designation is shown with m being the azimuthal quantum number in the limit of vanishing modulation [see Fig. 2(b) of Ref. 23]. The band gaps due to the periodic azimuthal modulation are indicated for the $n=0$ and $n=1$ families and $m=\pm 2$.

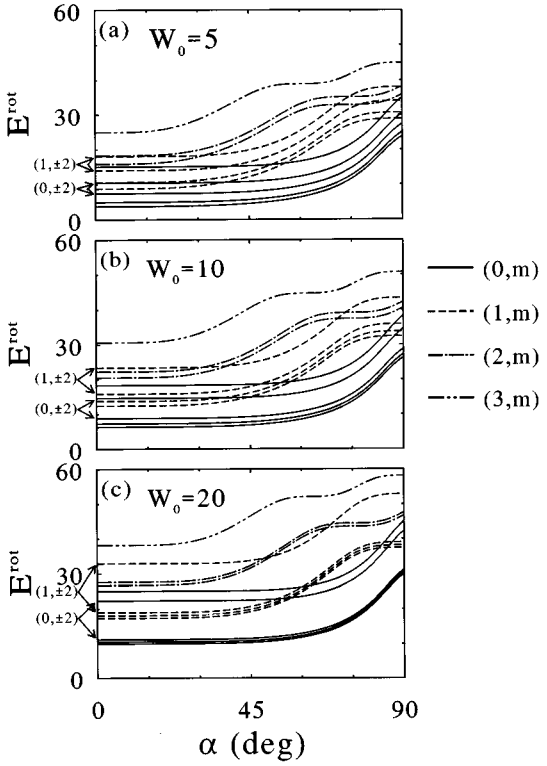

FIG. 6. Low-lying rotational energy levels (in units of $B=\hbar^2/2I$) of a horizontally hindered rotor [see Fig. 1(c) for $V_{\mathrm{II}}=0$, $V_{\mathrm{I}}=V_{\mathrm{III}}=20$, and $\beta=180°-\alpha$] as functions of the hindrance angle α (in degrees) for azimuthal modulation potential barrier heights (a) $W_0=5$, (b) $W_0=10$, and (c) $W_0=20$. The azimuthal modulation is sinusoidal with fourfold symmetry ($N=4$). The (n,m) designation is shown with m being the azimuthal quantum number in the limit of vanishing modulation [see Fig. 3(b)]. The band gaps due to the periodic azimuthal modulation are indicated for the $n=0$ and $n=1$ families and $m=\pm 2$.

One can expect that, as W_0 increases, the states approach harmonic-oscillator-like states, and as seen in Fig. 4, the levels of μ^2 tend toward equal spacing.

To investigate the effect of azimuthal modulation upon rotational levels, the low-lying energy levels of a modulated vertical rotor [see Fig. 1(a) for $V_{\mathrm{I}}=0$, and $V_{\mathrm{II}}=V_{\mathrm{III}}=20$] and a modulated symmetric horizontal rotor [see Fig. 1(c) for $V_{\mathrm{II}}=0$, $V_{\mathrm{I}}=V_{\mathrm{III}}=20$, and $\beta=\pi-\alpha$] for fourfold azimuthal symmetry [$N=4$ in Eq. (5)] for different modulation barrier heights, namely, $W_0=5$, 10, and 20 as functions of hindrance angle α are presented in Figs. 5 and 6, respectively. Figures 5 and 2(b) of Ref. 23 and Figs. 6 and 3(b) afford direct comparison between the results of the rotational energy levels with and without the azimuthal modulation. From these figures one can find that, for given values of N, the increasing of the barrier height W_0 yields increasing of μ^2 and, therefore, increases the energies of the rotational states. When $\alpha=\pi$ for the vertical configuration or $\alpha=0$ for the horizontal configuration, i.e., there is no restrictive cone, the energy of the rotational state within the nth family becomes $E^{\mathrm{rot}}=(|\mu_m|+n)(|\mu_m|+n+1)B$ from Eq. (20b). When the conical well reduces, E^{rot} increases oscillatorily as that in the unmodulated rotor cases. When α approaches zero for the vertical configuration or $\pi/2$ for the horizontal configuration, the rotor is nearly unhindered again; therefore, the energy becomes $E^{\mathrm{rot}}\approx(|\mu_m|+n)(|\mu_m|+n+1)B+VB$, where $V=V_{\mathrm{II}}$ for the vertical rotor or $V=V_{\mathrm{I}}$ for the horizontal rotor. The banding of μ^2 with increasing W_0 as shown in Fig. 4 is reflected in the rotational energies displayed in Figs. 5 and 6. This banding is reflected within each of rotational state families. In Figs. 5 and 6, the splittings of $(0,\pm 2)$ and $(1,\pm 2)$ states are indicated. The band gaps due to the periodic azimuthal modulation increase as the modulation barrier is increased. The convergence of states into bands upon increasing modulation strength is clearly seen. That is, when the barrier height increases, the gaps becomes wider and the band becomes narrower.

C. Rotational-state distributions

Now consider the desorption problem. If the desorption is induced by a fast process, such as electron or photon bombardment or rapid heating, one can assume that the hindering potential is suddenly switched off, and that hindered-to-free rotational transition takes place without altering the wave function. In such sudden unhindrance approximation,[14–16]

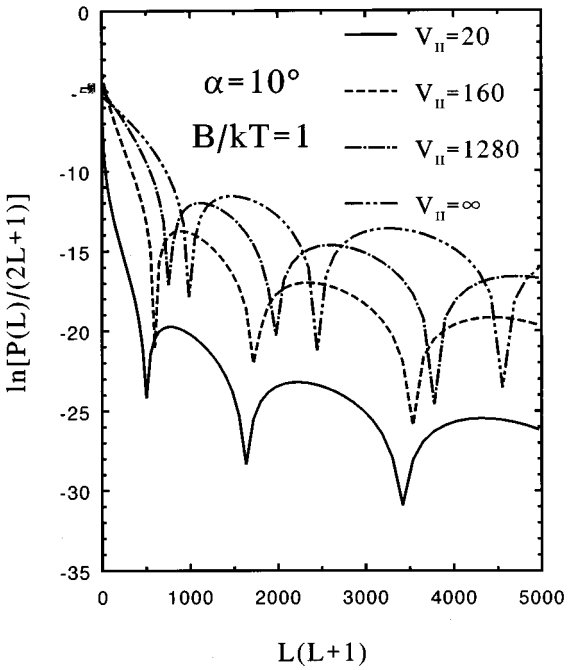

FIG. 7. Rotational-state distribution of the suddenly unhindered rotor of Fig. 1(a) for $V_{\mathrm{I}}=0$, $V_{\mathrm{II}}=V_{\mathrm{III}}=20$, 160, 1280, and ∞ with $\alpha=10°$ and $B/kT=1$, plotted in the form $\ln[P(L)/(2L+1)]$ vs $L(L+1)$.

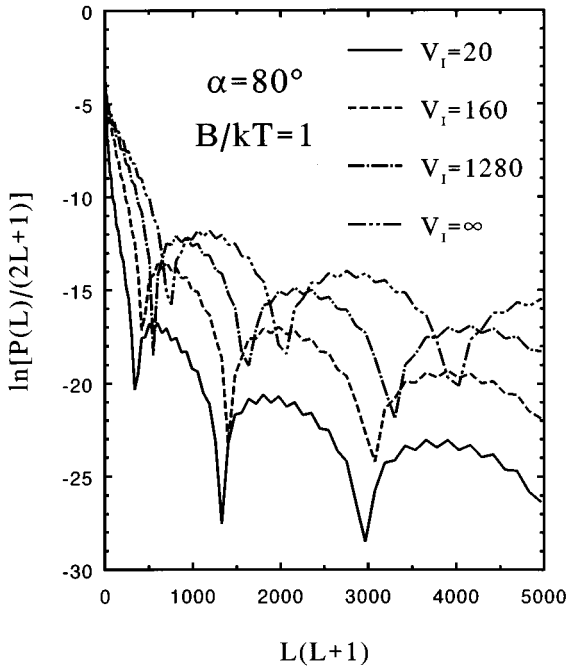

FIG. 8. Rotational-state distribution of the suddenly unhindered rotor of Fig. 1(c) for $V_{\mathrm{II}}=0$, $V_{\mathrm{I}}=V_{\mathrm{III}}=20$, 160, 1280, and ∞ with $\alpha=80°$, $\beta=180°-\alpha$, and $B/kT=1$, plotted in the form $\ln[P(L)/(2L+1)]$ vs $L(L+1)$.

the population of free-rotational states when molecules are quickly desorbed from the surface can be calculated.

The free-rotational states are described by a set of spherical harmonics: $\{Y_{L,M}(\theta,\phi)\}$; thus the probability of ending up in the Lth free-rotational state is the sum of rotational Franck-Condon factors between the final state $Y_{L,M}$ and the hindered-rotational state $\Psi^{\mathrm{rot}}_{v,\mu}$ weighted by appropriate thermal factors; that is,

$$P(L)=\frac{1}{Z_{\mathrm{hin}}}\sum_{M,v,\mu}\exp[-B\nu(\nu+1)/kT]|\langle Y_{L,M}|\Psi^{\mathrm{rot}}_{v,\mu}\rangle|^2, \tag{23}$$

where T is the surface temperature, k is the Boltzmann constant, and Z_{hin} is the partition function of the hindered rotor. In Eq. (23), we have assumed the center of mass of the molecule to be always at rest, i.e., no center of mass translational energy, and consider only the purely hindered-to-free rotational transition.

The calculated final rotational-state distributions based on Eq. (23) with $B/kT=1$ for various potential barrier heights are shown in Figs. 7 and 8. Figure 7 presents the result for the vertically hindered rotor [see Fig. 1(a)] while Fig. 8 is for the horizontally hindered rotor [see Fig. 1(c)]. For convenience, in our calculation, we have neglected the modulation potential, i.e., setting $W(\phi)=0$. As the conventional treatment, we plot the curves of $\ln[P(L)/(2L+1)]$ vs $L(L+1)$. It is known that for a Boltzmann distribution a straight line with slope $=-B/kT$ should be obtained. However, from Figs. 7 and 8, one can note that the rotational-state distributions are significantly influenced by the hindering potential and a non-Boltzmann feature is obtained.

In Figs. 7 and 8, the calculated final-state distributions exhibit two different behaviors. For the low-L region a nearly linear behavior is seen in which an effective rotational temperature T_r can be determined by equating the slope to $-B/kT_r$. One can note that, the greater the potential strength, the higher the effective rotational temperature T_r can be obtained. Furthermore, the effective temperatures T_r for all of hindrance conditions are higher than the surface temperature T. This rotational heating effect[14–16] has been found in the electron-stimulated desorption experiment,[22] and can be realized by the fact that, at low enough temperature, the final free-rotational-state distribution is due to the conversion of initial-state zero-point energy, not thermal excitation. A higher potential-barrier height yields greater initial-state zero-point energy; therefore, a higher effective rotational temperature T_r can be obtained. This also explains the fact that the probability of an unhindered rotor appearing in the high-L region for a greater hindering potential strength is greater than that for smaller hindering potential strength. This is due to the fact that, at low enough temperature, the hindered rotor is primarily located at low-lying states. Thus the population of the final high-L states depends mainly on their overlaps with the low-lying ν states. When we gradually increase the strength of the hindering potential, energies of the low-lying ν states start to increase, and the overlaps of the low-lying ν states with the high-L states become more prominent.

For the high-L region, the curves in Figs. 7 and 8 display qualitatively different behavior from that of the curves in the low-L region. At some critical L value, the state distribution drops precipitously from the linear form, then rises to form a plateau. Such alternate drops and plateaus make the state

distribution an oscillatory structure. The oscillations show a periodicity in L as $180°/\alpha$ for the vertical rotor and $180°/(90°-\alpha)$ for the symmetric horizontal rotor. This oscillatory structure can be understood as follows: For the high-L region, the rotational Franck-Condon factors between the final state $Y_{L,M}$ and the hindered-rotational state $\Psi^{\rm rot}_{v,\mu}$ oscillate as L increases. When the Franck-Condon factors are summed over different M, ν, and μ weighted by the appropriate Boltzmann factors, they form precipitous drops and plateaus. The plateau structure was observed in a gas-surface scattering experiment, and was interpreted in terms of rotational rainbows.[48] This implies an intimate connection between the rotational rainbows and the molecule-surface interaction.

In Fig. 8, the calculated rotational-state distributions for the horizontally hindered rotor show that in addition to the oscillatory structures there are zigzags along the curves. These zigzags occur because the horizontally hindering potential is chosen to be symmetrical with respect to the $\theta=\pi/2$ plane, and thus the hindered rotational state $\Psi^{\rm rot}_{v,\mu}$ bears the definite parity. The dominant ground state is even. Therefore, the Franck-Condon factors between the odd-L free-rotational state and the ground hindered state should vanish. One can find that the zigzag is minimum at odd L and maximum at even L. One can expect that the zigzag structure will disappear when the surface temperature is very high. This is because at high temperature the ground state is no longer dominant.

To investigate the oscillation of Franck-Condon factor, one can recall the analogy between the hindered-rotor problem and the Kronig-Penney model problem.[23] The Cartesian-coordinate counterpart of the free rotor states $Y_{L,M}$ are the following free-particle states which satisfy periodic boundary condition $\Psi(x+2\pi)=\Psi(x)$:

$$\Psi^{\rm free}_{{\rm even},N}(x)=\begin{cases}\dfrac{1}{\sqrt{2\pi}}, & N=0\\[2ex] \dfrac{1}{\sqrt{\pi}}\cos(Nx), & N=1,2,3,\ldots\end{cases} \tag{24a}$$

for even states and

$$\Psi^{\rm free}_{{\rm odd},N}(x)=\frac{1}{\sqrt{\pi}}\sin(Nx), \quad N=1,2,3,\ldots \tag{24b}$$

for odd states. These wave functions have been normalized in the region of $-\pi\leqslant x\leqslant\pi$. For the infinite well case, i.e., $V_{\rm II}\rightarrow\infty$. Our vertical conical well [see Fig. 1(a) for $V_{\rm II}\rightarrow\infty$] corresponds to an infinite square well with width of 2α. The hindered particle states of such infinite square well are

$$\Psi^{\rm hin}_{{\rm even},n}(x)=\frac{1}{\sqrt{\alpha}}\cos\left(\frac{n\pi}{2\alpha}x\right), \quad n=1,3,5,\ldots \tag{25a}$$

for even states and

$$\Psi^{\rm hin}_{{\rm odd},n}(x)=\frac{1}{\sqrt{\alpha}}\sin\left(\frac{n\pi}{2\alpha}x\right), \quad n=2,4,6,\ldots, \tag{25b}$$

for odd states. Therefore, for a hindered-to-free transition the probability is

$$p^{n\rightarrow N}_{\rm even}=\begin{cases}\dfrac{8\alpha}{n^2\pi^2}, & N=0\\[2ex] \dfrac{n^2\pi}{\alpha^3}\left[\dfrac{\cos(\alpha N)}{N^2-(n\pi/2\alpha)^2}\right]^2, & N=1,2,3,\ldots\end{cases} \tag{26a}$$

for even-to-even transition or

$$p^{n\rightarrow N}_{\rm odd}=\frac{n^2\pi}{\alpha^3}\left[\frac{\sin(\alpha N)}{N^2-(n\pi/2\alpha)^2}\right]^2, \quad N=2,4,6,\ldots \tag{26b}$$

for odd-to-odd transition. One can easily find that the transition probability oscillates as N varies. The probability has drops at $N=s\pi/2\alpha$, $s=1,3,5,\ldots$ for even-to-even transition or $s=2,4,6,\ldots$ for odd-to-odd transition [except $N=n\pi/2\alpha$, where $\Psi^{\rm free}_N(x)$ and $\Psi^{\rm hin}_n(x)$ specify the same states in the well region]. Therefore the spacing between two neighbor drops is just $\Delta N=\pi/\alpha$. Examining the free-particle states $\Psi^{\rm free}_N$ with $N=s\pi/2\alpha$, one can find $\Psi^{\rm free}_N$ states are just the states which are orthogonal with $\Psi^{\rm hin}_n$.

For the finite vertical conical well, its Cartesian counterpart is just a set of periodic square wells. The hindered particle states are now the zone-center Bloch states. A similar treatment will deduce an oscillatory hindered-to-free transition probability. The spacing between two neighbor drops of the probability is also $\Delta N=\pi/\alpha$. On the other hand, a similar treatment of the Cartesian counterpart of a horizontal conical well potential will deduce an oscillatory hindered-to-free transition probability with periodicity $\Delta N=\pi/(\pi/2-\alpha)$.

From the above simple comparison between the hindered rotor problem and its Cartesian-coordinate counterpart, one can conclude that the oscillation of the Franck-Condon factors is a general result of a system transiting from hindered states to free states. The drops of the Franck-Condon factors occur when the final free states are orthogonal (or nearly orthogonal) with the initial hindered states. The periodicity of the oscillation is related to the geometry structure of the hindering potential. The oscillation of the Franck-Condon factor reflects the rotational invariance of the hindered rotor problem.

One can determine the parameters of the model potential function by fitting the calculated rotational-state distribution to the measured distribution. Figure 9 shows the measured distributions for CN* desorbed form the Li and Cs surfaces,[22] and the calculated results of Ref. 22 and us by least-squares fitting. In the calculation of Ref. 22, the hindering potential was modeled as a complicated form with three parameters. In our calculation, the potential was modeled as a vertical conical well as shown in Fig. 1(a). For the soft-wall conical well, the cone opening angle α and the potential barrier height $V_{\rm II}$ were set as parameters, while for the hard-wall conical well, only α was a parameter. In the fitting calculations, the model potential was assumed to be ϕ independent and only the ground initial state was considered due to the low substrate temperature.

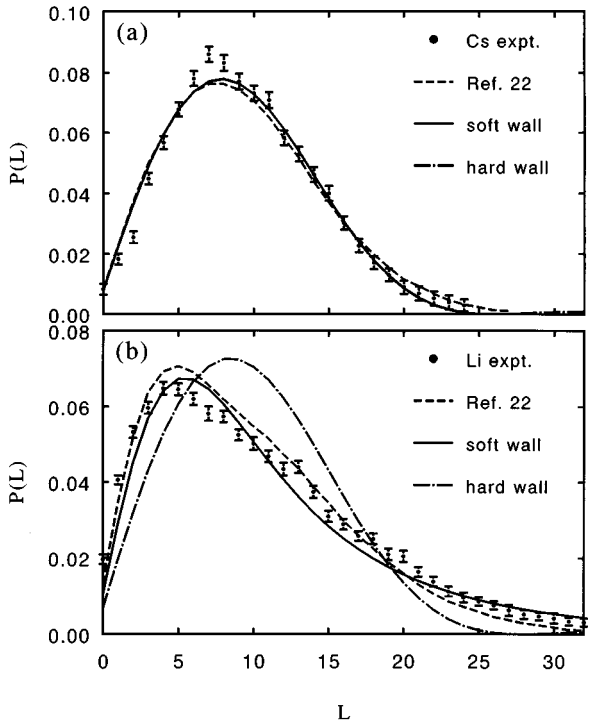

FIG. 9. Comparisons of the calculated rotational distribution with measured distribution: (a) for CN* desorbed from the Li surface, and (b) for CN* desorbed from the Cs surface (Ref. 22).

The fitted parameters of both soft- and hard-wall conical wells are presented in Table I. As shown in Table I, surface hindering potential depends strongly on the substrates. The potential barrier height for the Cs surface is very large; therefore, as shown in Fig. 9, our calculated results for both finite and infinite conical wells are nearly coincident with each other, and these results are in agreement with the results of Ref. 22. On the other hand, the potential barrier height for the Li surface is smaller, and therefore the hard-wall conical well induced a poor result; however, the soft-wall well induced a better one.

From Table I, one can note that the finite conical well for the Li surface has a very small cone opening angle, while that for the Cs surface has a larger one. This agrees the fitted result of Ref. 22. The small cone opening angle for the Li surface confines a CN molecular wave function in a small-angle region, and renders a large zero-point energy. Therefore, when CN is desorbed, more energy is transferred into the final rotational states for the Li surface than those for the Cs surface, and the distribution for CN desorbed from Li is wider than that for CN desorbed from Cs. Figure 9 shows this result.

TABLE I. The fitted parameters of the vertical soft- and hard-wall conical wells for Cs-CN and Li-CN adsorption systems.

	Cs-CN		Li-CN	
conical well	α (degree)	V_{II} (eV)	α (degree)	V_{II} (eV)
soft wall	11.36	2.45	1.85	0.31
hard wall	12.01	∞	11.2	∞

Finally, some comments on the difference between the soft- and hard-wall conical wells are made. As we showed above, the rotational levels of a soft-wall-hindered rotor exhibit oscillatory behavior. This is absolutely different from that of a hard-wall rotor. Further, the infinite-conical-well model potential is suitable only for the adsorption system with a large potential barrier height; however, the finite one is suitable for most of adsorption system due to the adjustable potential barrier heights. This is very helpful to estimate the interaction strength between adsorbed molecules and surfaces by fitting experimental data. Above, we showed that our fitted rotational-state distributions for the finite-conical-well model are in agreement with the previously measured and calculated distributions. However, the infinite-conical-well model gives poor results for a system with a small potential barrier height.

Another advantage of the finite-conical-well model is that as the role of finite square well in the Cartesian space, the finite conical well plays a basic role in the polar space. Any complicated hindering potential in the polar space can be approximated by a series of suitable finite wells or barriers, and the mathematical treatment is just the extension of our above treatments. However, an infinite well is useless to approximate most of complicated hindering potential.

It is possible for some adsorption systems that the hindering potential has minima about $\theta=0$ and $\pi/2$, i.e., that both vertical and horizontal adsorption configurations are stable. One can expect that if the potential barrier height is not very large, an exchange between two different adsorption configurations is possible due to the tunneling effect or external perturbations. One can investigate such vertical-horizontal exchange by applying the finite-conical-well model. However, the infinite-conical-well model is useless because it precludes completely the transition probability.

IV. CONCLUSIONS

We have studied the hindered and modulated rotational motion of an adsorbed diatomic molecule. Both vertical and horizontal adsorption configurations were studied, respectively, by modeling the surface potentials as solvable vertical and horizontal finite conical wells. In addition to the polar hindrance, we studied the effect of the azimuthal modulation upon the rotational energy levels. The azimuthal modulation was assumed to possess the local symmetry of the adsorption site.

The calculated rotational energies increase as the region of the conical well is reduced. They also show an oscillatory behavior when they are plotted as functions of the hindrance angle. The physical origin of the oscillatory behavior can be ascribed to the phenomenon of the resonance transmission. By examining variations of rotational levels, one can classify energy levels into different families in accordance with n, which is the number of nodes of molecular polar wave function.

The effect of increasing modulation barrier height upon the azimuthal quantum number μ^2 was found. The results exhibited the progressive splitting of μ^2 for m at the Brillouin-zone edge and the banding effect of μ^2 as the height of the azimuthal barrier W_0 increases. This banding effect is reflected within each rotational level family. The

levels within each family were found to converge into bands as the modulation strength increases.

By employing the sudden unhindrance approximation, the solutions of the hindered molecules were used to calculated the rotational-state distributions of molecules desorbed from a solid surface. When the calculated state distributions were plotted semilogarithmically, two distinctly different regimes appeared. For the low-L region a nearly linear behavior was seen in which an effective rotational temperature T_r can be determined. T_r was found to be independent of the surface temperature. On the other hand, the high-L region displayed an oscillatory structure with alternate drops and plateaus. The oscillation structure is a general result of a system transiting from hindering states to free states, and can be regarded as the manifestation of the rotational invariance. The calculated state distributions were used to fit the previously measured data, and the parameters of the hindering potential were obtained. For an adsorption system with a smaller potential barrier height, only the results of the finite-conical-well model agree with the measured data.

ACKNOWLEDGMENT

This work was supported by the National Science Council, Taiwan, Republic of China.

*Author to whom all correspondence should be addressed.
[1] J. S. Koehler and D. M. Dennison, Phys. Rev. **57**, 1006 (1940).
[2] K. S. Pitzer and W. D. Gwinn, J. Chem. Phys. **10**, 428 (1942).
[3] *Internal Rotation in Molecules*, edited by W. J. Orville-Thomas (Wiley, New York, 1974).
[4] S. W. Benson, *Thermochemical Kinetics*, 2nd ed. (Wiley, New York, 1976), pp. 91, 92, and 161–166.
[5] P. D. Pacey, J. Chem. Phys. **77**, 3540 (1982).
[6] L. Pauling, Phys. Rev. **36**, 430 (1930).
[7] R. F. Curl, Jr., H. P. Hopkins, Jr., and K. S. Pitzer, J. Chem. Phys. **48**, 4064 (1968).
[8] H. Kono and S. H. Lin, J. Chem. Phys. **78**, 2607 (1983).
[9] Y. L. Sandler, J. Phys. Chem. **58**, 58 (1954).
[10] D. White and E. N. Lassettre, J. Chem. Phys. **32**, 72 (1960).
[11] A. L. Myers and J. M. Prausnitz, Trans. Faraday Soc. **61**, 755 (1965).
[12] M. P. Freeman and M. J. Hagyard, J. Chem. Phys. **49**, 4020 (1968).
[13] I. F. Silvera and M. Nielsen, Phys. Rev. Lett. **37**, 1275 (1976).
[14] J. W. Gadzuk, U. Landman, E. J. Kuster, C. L. Cleveland, and R. N. Barnett, Phys. Rev. Lett. **49**, 426 (1982).
[15] U. Landman, Isr. J. Chem. **22**, 339 (1982).
[16] J. W. Gadzuk, U. Landman, E. J. Kuster, C. L. Cleveland, and R. N. Barnett, J. Electron Spectrosc. Relat. Phenom. **30**, 103 (1983).
[17] U. Landman, G. G. Kleiman, C. L. Cleveland, E. Kuster, R. N. Barnett, and J. W. Gadzuk, Phys. Rev. B **29**, 4313 (1984).
[18] V. M. Allen and P. D. Pacey, Surf. Sci. **177**, 36 (1986).
[19] M. D. Alvey, J. T. Yates, Jr., and K. J. Uram, J. Chem. Phys. **87**, 7221 (1987).
[20] S. Krempl, Surf. Sci. **259**, 183 (1991).
[21] D. J. Dai and G. E. Ewing, J. Chem. Phys. **98**, 5050 (1993)
[22] J. Xu, A. Barnes, R. Albridge, C. Ewig, N. Tolk, and L. D. Hulett, Jr., Phys. Rev. B **48**, 8222 (1993).
[23] Y. T. Shih, D. S. Chuu, and W. N. Mei, Phys. Rev. B **51**, 14626 (1995).
[24] C. M. Cunningham and H. L. Johnston, J. Am. Chem. Soc. **80**, 2377 (1958).
[25] C. M. Cunningham, D. S. Chapin, and H. L. Johnston, J. Am. Chem. Soc. **80**, 2382 (1958).
[26] D. A. Depatie and R. L. Mills, Rev. Sci. Instrum. **39**, 105 (1968).
[27] Ph. Avouris, D. Schmeisser, and J. E. Demuth, Phys. Rev. Lett. **48**, 199 (1982).
[28] S. Andersson and J. Harris, Phys. Rev. Lett. **48**, 545 (1982).
[29] A. R. Burns, Phys. Rev. Lett. **55**, 525 (1985).
[30] A. R. Burns, E. B. Stechel, and D. R. Jennison, Phys. Rev. Lett. **58**, 250 (1987).
[31] R. R. Cavanagh and D. S. King, Phys. Rev. Lett. **47**, 1829 (1981).
[32] D. S. King, D. A. Mantell, and R. R. Cavanagh, J. Chem. Phys. **82**, 1046 (1985).
[33] D. A. Mantell, R. R. Cavanagh, and D. S. King, J. Chem. Phys. **84**, 5131 (1986).
[34] F. Frenkel, J. Häger, W. Krieger, H. Walther, C. T. Campbell, G. Ertl, H. Kuipers, and J. Segner, Phys. Rev. Lett. **46,** 152 (1981).
[35] A. W. Kleyn, A. C. Luntz, and D. J. Auerbach, Phys. Rev. Lett. **47**, 1169 (1981).
[36] D. Weide, P. Audresen, and H. -J. Freund, Chem. Phys. Lett. **136**, 106 (1987).
[37] G. O. Sitz, A. C. Kummel, and R. N. Zare, J. Chem. Phys. **89**, 2558 (1988).
[38] B. H. Choi, Z. B. Guvenc, and N. L. Liu, Phys. Rev. B **42**, 3887 (1990).
[39] P. M. Morse and H. Feshbach, *Methods of Theoretical Physics* (McGraw-Hill, New York, 1953), Vol. 1.
[40] *Higher Transcendental Functions*, edited by A. Erdelyi (McGraw-Hill, New York, 1953), Vol. I.
[41] *Handbook of Mathematical Functions*, edited by M. Abramowitz and I. A. Stegun (Dover, New York, 1970).
[42] M. Grunze, P. A. Dowben, and R. G. Jones, Surf. Sci. **141**, 455 (1984).
[43] D. Mueller, T. N. Rhodin, and P. A. Dowben, Surf. Sci. **164**, 271 (1985)
[44] J. W. Riehl and C. J. Fisher, J. Chem. Phys. **59**, 4336 (1973).
[45] R. P. Pan, R. D. Etters, K. Kobashi, and V. Chandrasekharan, J. Chem. Phys. **77**, 1035 (1982).
[46] E. Merzbacher, *Quantum Mechanics*, 2nd ed. (Wiley, New York, 1970).
[47] L. D. Landau and E. M. Lifshitz, *Quantum Mechanics*, 3rd ed. (Pergamon, New York, 1977).
[48] R. Schinke, J. Chem. Phys. **76**, 2352 (1982).